DOI: 10.13009/EUCASS2025-710
11TH EUROPEAN CONFERENCE FOR AERONAUTICS AND SPACE SCIENCES (EUCASS)

From design to additive manufacturing: Advancing a LOX/Methane clustered aerospike engine segment towards experimental validation

Jan Sieder-Katzmann[a†], Florian Ditsche[a], Wolfgang Armbruster[e], Wojciech Florczuk [f], Justin Hardi [e], Daniel Heußen [c], Dominik Kublik [f], Tim Lantzsch [c], Martin Propst [a], Ralf Stark [e], André Seidel [g], Uwe Teicher [d], Simon Hyde [b], Martin Tajmar[a,h] and Christian Bach[a]

[a] *TUD Dresden University of Technology,Institute of Aerospace Engineering,*
Chair of Space Systems, 01307 Dresden, Germany
[b] *European Space Agency (ESA), European Space Research and Technology Centre (ESTEC),*
Noordwijk, The Netherlands
[c] *Fraunhofer Institute for Laser Technology ILT, Aachen, Germany*
[d] *Fraunhofer Institute for Machine Tools and Forming Technology IWU, Dresden, Germany*
[e] *German Aerospace Center (DLR), Institute of Space Propulsion, Hardthausen, Germany*
[f] *Łukasiewicz Research Network - Institute of Aviation, Warszawa, Poland*
[g] *Seidel Consulting, Dresden, Germany*
[h] *Faculty of Space Technologies, AGH University of Krakow, Poland*
jan.sieder-katzmann@tu-dresden.de · https://tu-dresden.de/ing/maschinenwesen/ilr
[†]Corresponding author

Abstract

A 3-kilonewton segment of a clustered aerospike engine for sea-level testing is developed within the ESA-funded THOMAS project. The focus lies on the design methodology of the whole nozzle, especially non-circular exits of internal expansion nozzle modules, the transition of the flow to the spike surface and the flow interaction. Subsequently, the design for the test specimen is derived, of which the main components are constructed with the copper alloy CuCr1Zr using additive manufacturing. The corresponding test plan for the upcoming verification test campaign is presented, which gives an insight into the approach to measure heat load, surface pressure distribution and flow phenomena analysis in such complex flow regime.

1. Introduction

As of today, bell-shaped nozzles have been the predominant choice for expanding the vehicle propelling exhaust gases in launcher and space craft propulsion systems to increase thrust and performance. However, various alternative nozzle designs have been investigated to overcome the performance losses, which bell nozzles suffer in off-design ambient conditions through over- and under-expansion.[1–3] The aerospike nozzle is one of the alternative concepts with ambient pressure adaptation capability. It has therefore been investigated for an updated version of the Saturn V rocket in form of the J-2T-250K engine[4] and as main propulsion system for the X-33 Venture Star program in form of the XRS-2200 engine.[2]

Furthermore, aerospike nozzles offer unique geometrical advantages over traditional bell nozzle engines, allowing to significantly reduce engine length and overall size.[5] This feature is especially advantageous for space missions where optimization of mass and volume is paramount. In addition, with its compact design, aerospike engines offer multifunctional capabilities, particularly for lander applications. By integrating the engine into the lander's design, it can also function as a heat shield during atmospheric entry, providing a dual-purpose solution that further enhances the lander's efficiency and structural simplicity, as it is currently also investigated for launcher systems.[6,7]

Even in vacuum conditions, where the major advantage of ambient pressure adaptation is eliminated, aerospike nozzles can provide performance advantages over bell nozzles. Especially annular configurations are particularly

DOI: 10.13009/EUCASS2025-710

attractive due to their compact form factor and high expansion ratios, offering a balanced trade-off between performance and volume.[5,8,9] In case of the ESA Argonaut lunar lander, a 10 % payload increase potential has been shown.[10]

However, for engine designs with high expansion ratios above 100 and thrust levels below 30 kN, the widely investigated annular aerospike nozzle design with toroidal combustion chamber and solely external expansion (e.g. CALVEIN,[11,12] NASA Dryden's solid rocket flight trials,[13] Deadalus Astronautics,[14] NextAero,[15] Pangea's DemoP1[16] as well as TU Dresden's CFDμSAT[17] and ASPIRER engines[18,19]) faces substantial geometrical challenges. With an increase of the expansion ratio, the Prandtl-Meyer turning angle increases as well as the throat gap decreases substantially. While the first can be compensated with an inversely oriented internal expansion, the latter becomes quickly a manufacturing challenge in terms of gap accuracy and uniformity. To overcome this challenge, the combustion space is divided into individual, mostly cylindrical combustion chambers arranged in a cluster surrounding the central spike. Examples for clustered aerospike engines are the linear XRS-2000[2] and the annular designs of RocketStar,[20] Pangea's ARCOS engine,[21] CALVEIN Prospector 10[22] and Firefly Alpha.[23] These clustered aerospike engines offer the capability of thrust vector control through differential throttling of the individual combustion chambers.[24,25] However, finding a design for the transition from internal expansion of the individual chambers to a combined external expansion on the spike without significant losses due to interacting shock systems remains challenging.

Aiming to answer some of these technical questions, the European Space Agency (ESA) is funding the THOMAS (THrottable Oxygen Methane AeroSpike) project (Ref: 4000142001/23/NL/MG), in which a clustered aerospike engine design for lander applications using methane and liquid oxygen as propellants is investigated. Furthermore, a sub-scale engine is developed, going to be manufactured and tested to investigate key aspects such as the design methodology and feasibility of additive manufacturing of a clustered aerospike engine. This particular test engine is designed for $3 - 4$ kN thrust. The major components (internal expansion nozzle(s) and spike) with included cooling channels will be additively manufactured using the copper alloy CuCr1Zr by a laser powder bed fusion process. Further focus of the project lies on the determination of thermal loads and flow phenomena of the test engine, especially in the transition zone from internal to external expansion. The final experimental investigation will be conducted a concluding hot run test campaign, which will be conducted at the German Aerospace Center (DLR) site in Lampoldshausen. This project is part of the overall effort at TUD Dresden University of Technology to overcome the low TRL and the following uncertainties associated with aerospike rocket engines and is carried out in cooperation with Fraunhofer IWU, Fraunhofer ILT, the Łukasiewicz Institute of Aviation and the German Aerospace Center (DLR).

Section 2 describes the development of the test specimen design. Starting with the boundary conditions implied by the envisaged test bench and considerations with respect to the general design, the detailed nozzle design procedure is presented. With the final design derived, the measurement approach and test plan conclude this section. The following section 3 explains the manufacturing strategy for the additively manufactured components of the test specimen and the current status of manufacturing. At last, the test and verification approach of the test specimen is decried in section 4 before concluding this contribution.

2. Design development of the test specimen

The goal of the sub-scale engine or test specimen is an overall technology demonstration of an additively manufactured aerospike engine from copper-alloy using methane and oxygen as propellants. It shall represent a high expansion version of this engine type for potential lander applications with a cluster of combustion chambers and non circular nozzle exits pre-expandign the flow internally. The associated experimental focus lies on the validation of the methodology used to design the test specimen, the investigation of flow interaction of the internally pre-expanded gases with the aerospike and their neighboring flows, the investigation of throttling, the proof of concept and heat load investigation.

Based on these goals, a very suitable test bench-combustion chamber combination has been selected as a basis for the specimen design development, which is described in this section. Starting with general design considerations, the details of the nozzle components design follows. Subsequently, the final design and operating conditions of the specimen are presented. At last, the measurement approach and test plan to tackle the above mentioned goals are explained.

2.1 Test bench & combustion chamber

The envisaged experimental verification of the test specimen will be conducted at the test bench P6.1 of the DLR Institute of Space Propulsion in Lampoldshausen. The test position P6.1 is designed for sub-scale thrust chamber hot-

DOI: 10.13009/EUCASS2025-710

fire testing with the cryogenic propellant combinations oxygen-hydrogen or oxygen-methane. It provides a maximum mass flow rate of about 1.5 kg/s and a chamber pressure up to 6.0 MPa.[26]

With the main focus of this project being the design and analysis of the aerospike nozzle, it was decided to make use of already existing and tested hardware of DLR to provide the desired gas flow into the nozzle. Hence, the aerospike nozzle test specimen will be combined with an existing injector head and cylindrical combustion chamber segments. Sender et al.[27] summarizes the different existing research thrust chambers available. For this project, chambers with an inner diameter of 50 mm (designated BKA, BKB and BKE) are best suited for the testing at P6.1. Based on a modular design, the injector heads and chamber segments of these specimen are interchangeable to a certain extent. One of these chambers is shown in fig. 1.

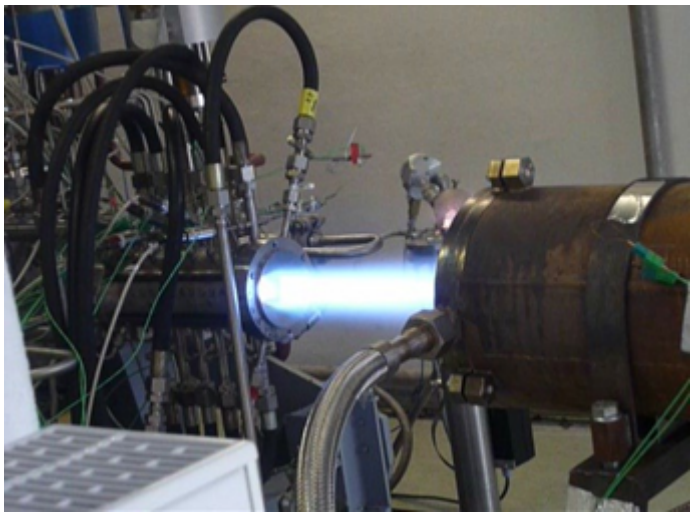

Figure 1: DLR combustion chamber firing at P6.1[27]

The envisaged injector head for this study consists of 15 shear coaxial elements. It has already been extensively tested with both LOX/H2 and LOX/CH4. An oxygen-hydrogen torch igniter will be used to start the combustion process and it is placed at the center of the injector head. The chamber segments themselves are water-cooled using a copper-based liner. Further details on this hardware are published in the respective publications.[27–31]

2.2 General design considerations

The goal of the specimen tests is the conceptual investigation of an aerospike engine with high expansion ratio, which is additively manufactured from copper-alloy and using methane and oxygen. On the one hand the aim is an as high as possible transferability of the test results to a real lander application, on the other hand ground testing and the test bench are setting limitations. Hence, compromises have to be made with respect to certain goals, leading to the following considerations:

- **High expansion area ratio:** Considering the maximum chamber pressure of the test bench with (6 MPa) and a minimum exit pressure on the Aerospike of approx. 0.1 MPa to avoid recompression waves on the spike's surface, a maximum pressure ratio of 60 is chosen.
- **Cluster concept:** A clustered aerospike engine concept was chosen to represent a high expansion engine design. This means, multiple combustion chambers are placed around a common spike. The flow is pre-expanded in these chambers and gets further expanded along the spike. The nozzles used for the internal pre-expansion are from the convergent-divergent type.
- **Segmentation:** As the test bench limits the number on thrust chambers to one and the mass-flow rate to 1.3 $\mathrm{kg\,s^{-1}}$, the only feasible concept is testing a segment with a single running chamber. The interaction with running neighboring chambers will be simulated with symmetry boundaries in form of side plates. By adding a not-running chamber segment, the interaction of the flow with a deactivated chamber section could be analyzed as well.

DOI: 10.13009/EUCASS2025-710

- **Shape of the internal expansion nozzle:** In order to generate a quasi-homogeneous flow field of all individual chambers around the spike, which then is further expanded, the divergent part of the internal nozzle is designed in form of a circle ring segment. The edges are rounded, due to mechanical stability reasons, resulting in a banana-shape.
- **Thickness of the banana-shape:** As the throat of the nozzle is circular, the development of the cross-sectional shape slowly transforms from a circle to a banana-shaped cross-section at the exit. During this transformation, the height of the developing shape, the thickness of the banana, remains constant. Hence, the thickness equals the throat diameter.

Based on these considerations and test boundary conditions (summarized in tab. 1), the engine concept for the test specimen was developed.

Table 1: Design parameters for the test specimen

Parameter	Value	Dimension
Engine number	1	-
Total mass flow rate	1.3	kg/s
Max. chamber pressure	6	MPa
Mixture ratio (ROF)	3.2	-
Isentropic exponent	1.63	-
Molar mass	21.319	kg/mol
Total temperature	3326	K
Ambient pressure	0.1	MPa

Fig. 2 shows an initial concept of the test specimen with a twin chamber design using a rectangualar nozzle exit pre-expanding the flow before expanding it on the spike.

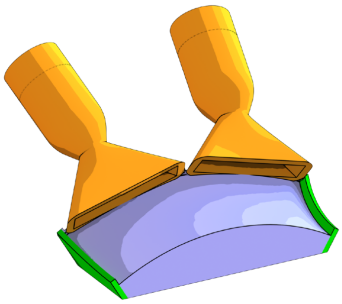

Figure 2: Concept of the test specimen with two combustion chambers

From the boundary conditions in tab. 1, the maximum performance can be calculated using ideal gas dynamics. This leads to a maximum thrust of $\approx 3.3\,\text{kN}$ for the segment. Moreover, the throat diameter from these values can be determined to 21.9 mm.

2.3 Detailed description of the nozzle design

Following the general design considerations, the details on the nozzle design are presented. Based on the spike contour, the transition area between internal and external expansion is determined. Subsequently, the contour of the internal nozzle is elaborated.

2.3.1 Segmentation

As described above, the test specimen represents only a segment of the virtual full clustered aerospike engine, as only one combustion chamber is to be used. By choosing a segment which represents the covered section by one engine (30 °-segment), the investigation of throttling behavior of the engine would be limited to mass flow throttling. By choosing a section which covers 1.5 clustered engines (45 °-segment) of which only one is running, a wider variety of

DOI: 10.13009/EUCASS2025-710

flow regimes can be investigated, as discussed in section 2.5.3.

2.3.2 Spike

To derive the segment, a full clustered aerospike engine is sketched, and later the segment is taken as a cut-out from this full engine. As this full aerospike engine will never be built, is called 'virtual full engine'. For the virtual full engine, an engine number of 12 is used, which offers a wide variety of throttling options through axial symmetric chamber shutdown. Hence, the virtual full engine has a total mass flow rate of $12 \cdot 1.3\,\mathrm{kg/s} = 15.6\,\mathrm{kg/s}$ and a total thrust of $12 \cdot 3.7\,\mathrm{kN} = 44.4\,\mathrm{kN}$. From these boundary conditions, the ideal Aerospike contour can be derived, with the Angelino method .[32] This delivers the contour for a completely external expanding ideal Aerospike with an annular throat, as a reference case (cf. fig. 3). The spike contour of the clustered virtual full Aerospike engine can be derived from this contour.

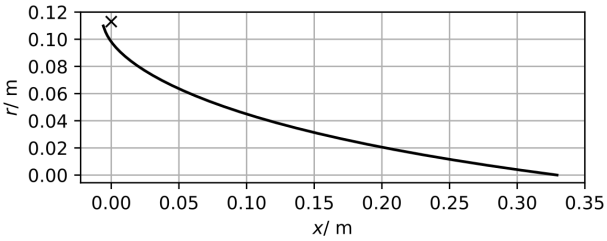

Figure 3: Contour of the ideal, fully externally expanding aerospike nozzle

The spike contour for the test specimen is truncated to 40 % of its ideal length to overcome the many disadvantages of the complete ideal spike. For example would the sharp tip at the end be very difficult to cool. This could be done, as a truncation to 20-30% of the ideal length will lead to comparably low performance losses.[33] The upstream occurring contour gap between spike and internal expansion nozzle, described with the following transition region, was closed with a spline in the CAD model. The spline was designed to connect tangentially to the nozzle and spike contour.

2.3.3 Transition - internal external expansion

At a certain point during the flow expansion of clustered aerospike engines, the transition from internal to external expansion is essential. In order to minimize the generation of strong and complex shock systems, the contour transition from internal to external expansion must be smooth and harmonized. Hence, the flowing considerations have led to the following modeling approach:
The initial assumption is that the flow from the internal expansion has the exact same parameters (Ma-number, pressure ratio, cross sectional area etc.) as it would have, if it has been expanded through an annular internal expansion. That means, that the flow transits homogeneously onto the spike through a continuous area without any gap (blue dotted line in fig. 4). This area has the shape of a truncated cone and starts at the outer expansion point R_E from the aerospike, the starting point of the Prandtl-Meyer expansion fan, and ends on the modified spike surface with radius r.

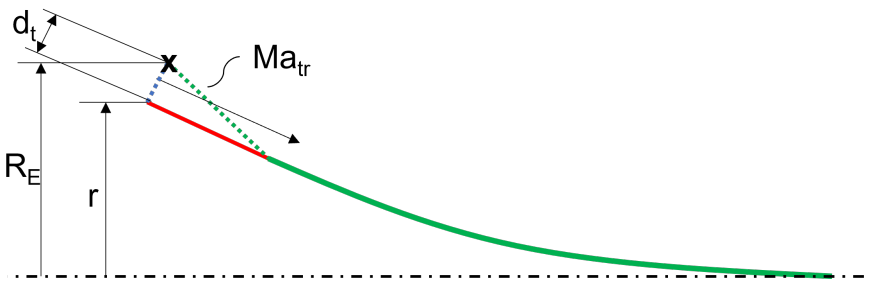

Figure 4: Cross-sectional scheme of the Spike contour: external expansion (green solid line) and transition contour(red solid line), Mach line of the transition Mach number (green dotted line), ideal conical area of the internal nozzle exit (blue dotted line)

DOI: 10.13009/EUCASS2025-710

In order to determine the corresponding transition Ma number, the equivalence between the truncated cone area $A_{e,int}$, the exit area of internal expansion, and the expansion area $A_{id.exp}(Ma)$ derived from the ideal expansion gas equations is identified. The former can be calculated using the equation:

$$A_{e,int} = (R_E + r)\,\pi\,d_t \tag{1}$$

where the value for r is derived via geometry from the expansion lines of the spike contour and the corresponding Mach angle. The latter cross sectional area $A_{id.exp}(Ma)$ is calculated with the isentropic exponent κ:

$$A_{id.exp}(Ma) = A_t \frac{1}{Ma}\left[\left(\frac{2}{\kappa+1}\right)\left(1+\frac{\kappa-1}{2}Ma^2\right)\right]^{\frac{\kappa+1}{2(\kappa-1)}} \tag{2}$$

with the throat area A_t of the full virtual engine:

$$A_t = 12\frac{\pi}{4}d_t^2 \tag{3}$$

The graphs of both areas in dependence on the Ma-number are plotted in fig. 5 in dependence of the Ma-number. Hence, the transition Mach number in that simplified case can be derived to $\mathrm{Ma}_{tr,end} = 2.38$, which is equivalent to the initial contour mach number of the spike. The exit Mach number of the inner expansion nozzle starting the transition region is smaller, as the banana-shaped nozzle does not fulfill perfectly the assumption to create a continuous flow-area. Furthermore, the individual nozzle wall thickness has to be taken into account. As the banana-shaped area needs to be wider as a segment of the ideal truncated cone. Hence, the initial transition Mach number was iteratively reduced to $Ma_{tr,init} = 2.15$ to fit the nozzles around the spike. Consequently, the transition Mach number range is spanning from $Ma_{tr,init} = 2.15$ to $Ma_{tr,end} = 2.38$.

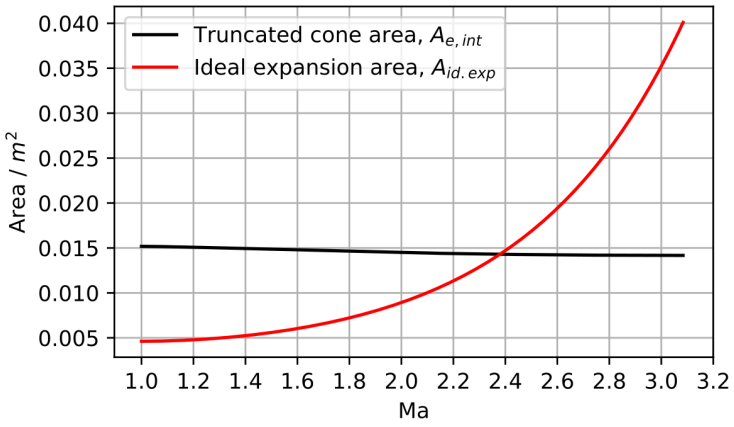

Figure 5: Truncated cone ($A_{e,int}$) and ideal expansion area $\left(A_{id.exp}(Ma)\right)$ in dependence of the Mach number

2.3.4 Banana-shaped Nozzle

The banana-shaped nozzle expands the flow internally to the transition pressure ratio. Subsequently, the exhaust gases expand from the outer lip - simultaneously the spike expansion radius - along the spike contour. The goal is to generate, in cooperation with all clustered nozzles together, an as continuous as possible flow that transits on to the spike.
For the derivation of the contour, an axial symmetric, truncated ideal contour (TIC) was generated via Rocket Propulsion Analysis (RPA)[34] using the boundary conditions presented in tab. 1.

The banana-shaped nozzle is derived with the same cross-sectional area evolution along the axis like the TIC nozzle ($A_{Banana}(x) = A_{TIC}(x)$). The convergent part remains unchanged axial symmetric. The shape of the banana-shaped cross-sections in the divergent part consists in general of three segments: two semicircles at the nozzle edges and the connecting circular ring segment, as shown in fig. 6

The area of the two semicircles equals the area of the throat (A_t), as they have the same diameter d_t. This is a direct result of the requirement that the "thickness" of the banana-shaped area shall keep the same height as the throat.

DOI: 10.13009/EUCASS2025-710

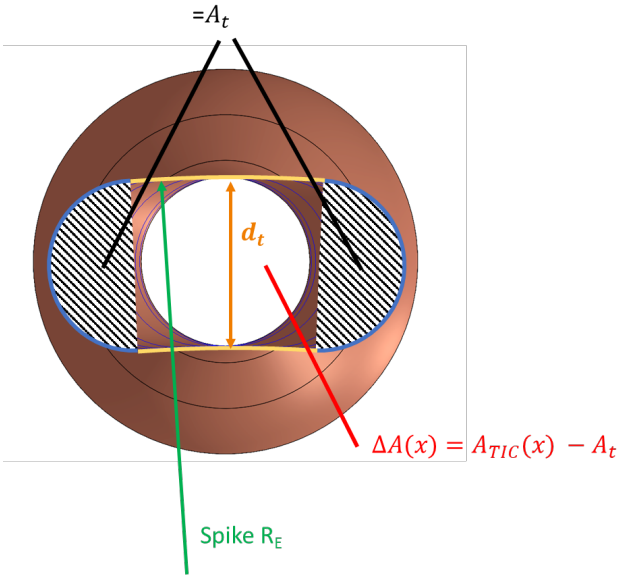

Figure 6: Scheme of area divison in cross-sectional area of the banana-shaped nozzle

As $A_{Banana}(x)$ increases with axial position, the ring segment of the banana shape $\Delta A(x) = A_{TIC}(x) - A_t$ increase as well. The curvature of the banana-shape is defined with the upper radius of the ring segment being set equal to the expansion radius R_E of the aerospike. With the description of the banana nozzle complete, the final specimen design can be derived. The design defining Mach numbers and pressure ratios of the test specimen are summarized in tab. 2.

Table 2: Nozzle design definition specifications

Nozzle data	**Transition** (internal/external)	**Truncation @40 %**	**Ideal spike:**
Area ratio ϵ	2.31 . . . 3.4	5.47	8.68
Pressure ratio	9.8 . . . 16.35	32.64	60
Ma-number	2.15 . . . 2.4	2.78	3.08

2.4 Final design and operating conditions

The test specimen itself consists of an internal expansion nozzle in shape of a banana, the external expansion nozzle (spike) and side plates, which ensure the rotational symmetry conditions. This nozzle set up (shown in Fig. 7) will be mounted to an existing combustion chamber provided by the DLR. A three-piece stainless steel mounting flange is used to connect the nozzle assembly to the DLR combustion chamber.

In order to ensure the durability of the test specimen, two cooling strategies are applied. Water cooling is applied for the additively manufactured internal expansion nozzle and the spike. The high thermally conductive copper alloy (CuCr1Zr) is used to ensure the required heat transport and therefore a remaining working temperature of the wall material below the maximum operating temperature (700 K, except the nozzle throat at maximum chamber pressure, which could reach $\approx$ 800 K) of these components. The side plates will utilize an ablative material, using the material S 5000® from Brandenburger. Under welding torch conditions, this material has an ablation rate of about 0.05 mm/s, which allows for sufficient testing time. Underneath the ablative material, stainless steel plates will ensure the mechanical stability.[35] Table 3 summarizes the operating conditions of the test specimen at the design point. It is designed such that the nozzle flow expands to an adapted flow to ambient pressure (p_{amb}) at the design operating conditions. A thrust loss of about 10 % with respect to the ideal number is assumed, based on the TIC-contour estimations derived in RPA.

DOI: 10.13009/EUCASS2025-710

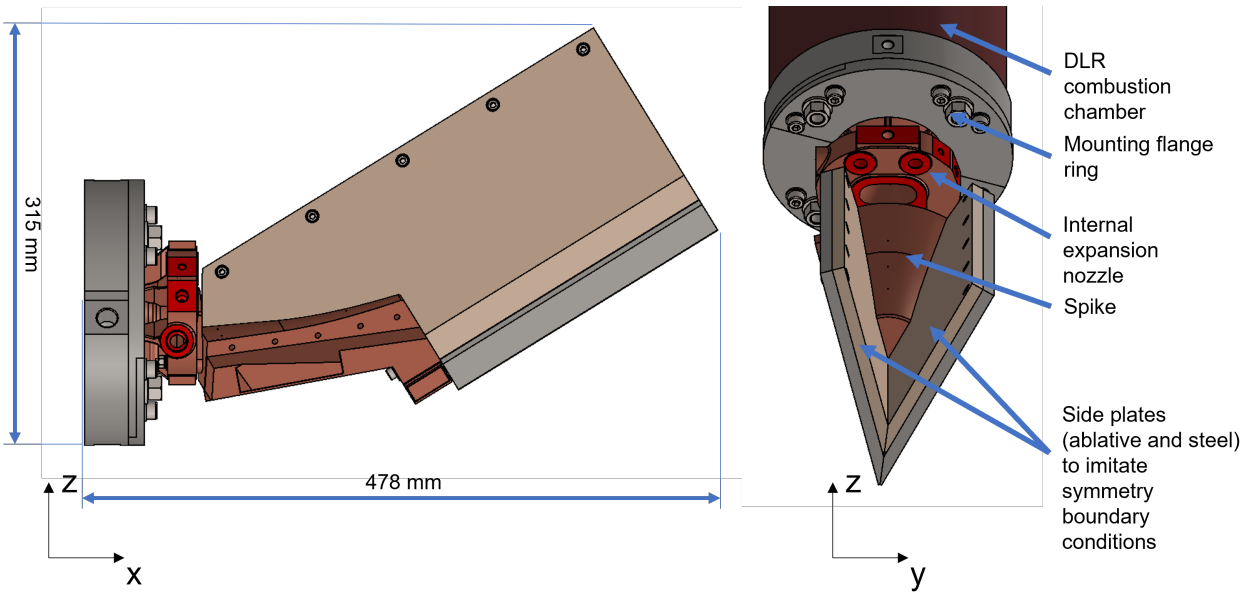

Figure 7: Test specimen side view with outer dimensions (left, front side plate hidden) and mounted to the DLR combustion chamber aft view (right)

Table 3: Operation conditions and design point specifications of the demonstrator

Parameter	Value
Chamber pressure p_0	6.0 MPa
Total pressure ratio p_0/p_{amb}	60
Chamber temperature T_0	3330 K
Nozzle exit Mach number Ma_e	3.08
Design thrust F	3.3 kN
Throat diameter d_t	21.9 mm
Total mass flow $\dot{m}$	1.3 kg/s
Fuel mass flow (CH4)	0.29 kg/s
Oxidizer mass flow (LOX)	0.94 kg/s
Mass flow ratio (ROF)	3.2
Coolant mass flow nozzle (H2O)	2 kg/s
Coolant mass flow spike (H2O)	1 kg/s

2.5 Measurement approach and test plan

The goal of the main test campaign in the THOMAS project is to investigate the operational and throttling behavior of a clustered aerospike engine with the presented test specimen. Throttling will be achieved via mass flow reduction and switching off individual combustion chambers. The operational behavior will be characterized through surface pressure measurements, optical flow phenomena analysis and calorimetric heat load measurements.

2.5.1 Surface pressure and optical flow phenomena

To assess the flow transition from internal to external expansion, the spike surface incorporates eleven surface pressure measurement probes to obtain the spike's surface pressure field. Furthermore, the flow phenomena in the proximity of the transition area shall be analyzed through visualization techniques. Schlieren systems, especially background oriented Schlieren systems (BOS), are planned for this application to enable flow visualization in radial and potentially in tangential direction. Especially the interaction of the expanding flow, leaving the internal expansion nozzle, with the central spike, the side fences as well as the ambiance are of interest. When the expanding flow reaches the solid surfaces of spike and side fences, significant and complex shock systems are to be expected.

DOI: 10.13009/EUCASS2025-710

2.5.2 Heat load

In order to measure the heat load on the entire nozzle surface, it will be equipped with pressure and temperature sensors in the cooling system. By measuring the change of the enthalpy of the coolant water between the in- and outlet (shown in Fig. 8), the integral heat load can be determined. Additional temperature sensors will be integrated into the spike, to analyze the temperature field within the component.

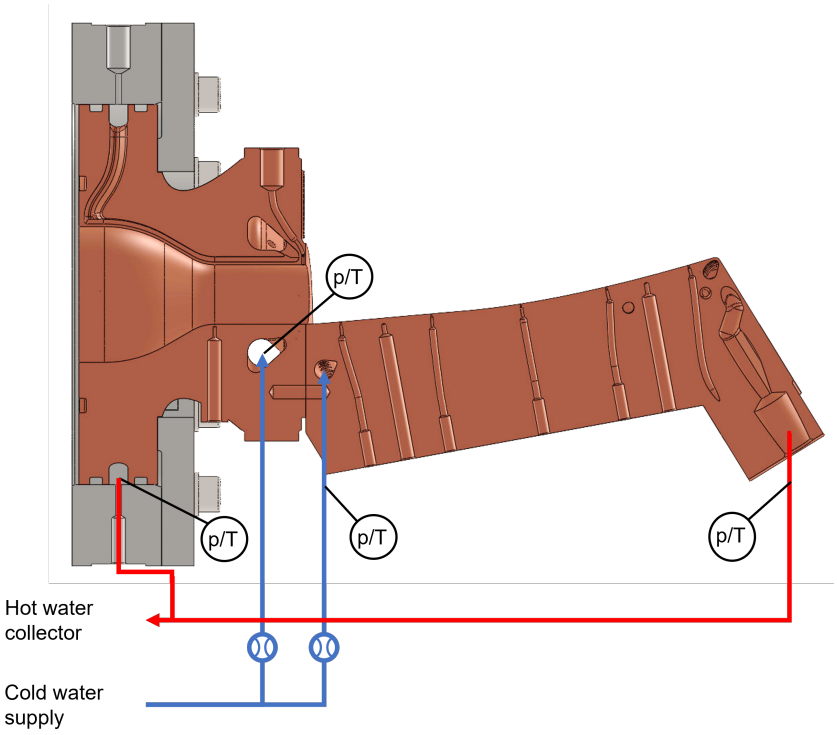

Figure 8: Schematic of the water cooling system for banana nozzle and spike with implemented heat load measurement approach

2.5.3 Throttling behavior analysis

The specimen, which represents a section of a virtual full spike, was designed in a way, that with a single test, multiple flow regimes on the spike surface are generated. These areas represent the characteristic flow regimes of different throttle conditions of a virtual full spike. Therefore, side fences were introduced to generate a symmetry boundary condition. Moreover, the actual demonstrator represents not one combustion chamber, but 1.5 combustion chambers from which only one is running. With this design, one side fence simulates the boundary condition of a running neighboring combustion chamber and the other simulates a shut down combustion chamber. This combination allows to create three flow regimes on the spike which represent different combinations of running and shut-off combustion chambers. Figure 9a - Fig. 9c show this in detail. The area depicted in blue in Fig. 9a represents the flow regime of a virtual full engine with all combustion chambers running. The blue area in Fig. 9b represents a virtual full flowing engine with every third combustion chamber shut down - equivalent to a throttling to 66 % thrust without reducing the chamber pressure. Figure 9c shows the area of interest which represent the flow regime in the case every second engine is switched off (50 % thrust).

In this way, already three flow regimes, which represent three throttling conditions, can be generated. By additionally varying the mass flow, three more regimes can be represented.
Therefore, it is foreseen to conduct tests with two different mass flows: 100 % and 50 % of the design mass flow. Table 4 shows the resulting throttling regimes, which can be generated by focusing on the respective areas.

DOI: 10.13009/EUCASS2025-710

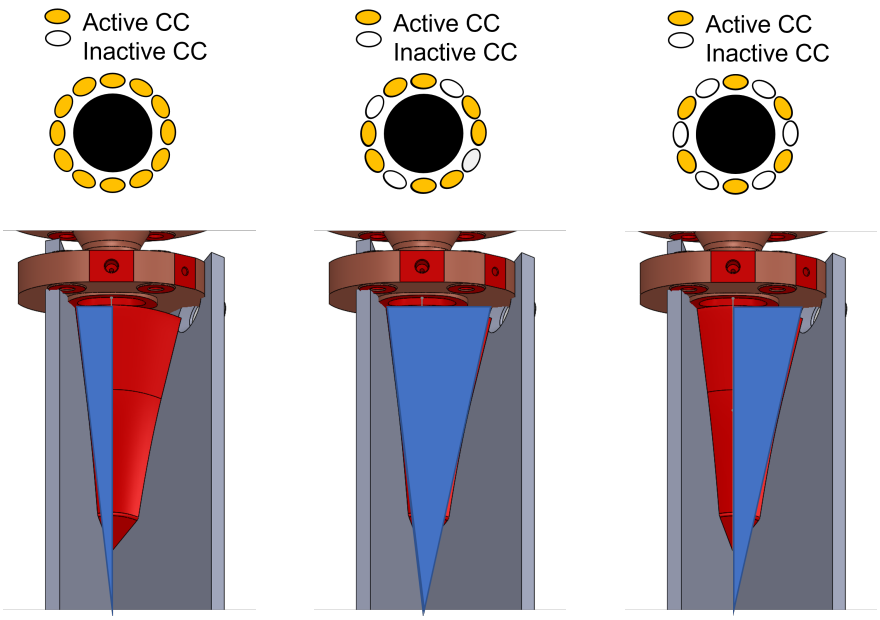

(a) All active (b) Two thirds active (c) One half active

Figure 9: Test concept for throttling via engine shut-down

Table 4: Overview of Throttling regimes

Representative Thrust Throttling regime	Flow regimes in breadboard demonstrator **Full flow (100%)**	**Two-thirds (67%)**	**Half flow (50%)**
100 % $p_{chamber}$	≈ 100 %	≈ 67 %	≈ 50 %
50 % $p_{chamber}$	≈ 50 %	≈ 33 %	≈ 25 %

3. Additive manufacturing of test specimen components

The additive manufacturing of the two components 'nozzle' and 'spike' using the copper alloy CuCr1Zr will be done in-house by the Fraunhofer (Fh) project partners. While the additive manufacturing itself is conducted at the Fh Institute for Laser Technology (ILT) in Aachen, Fh Institute for Machine Tools and Forming Technology (IWU) in Dresden will conduct the post processing, as described in the following manufacturing strategy. Following this strategy, first critical design elements have been manufactured and are currently investigated, preparing and tweaking the manufacturing for the test specimen components.

3.1 Manufacturing strategy

Due to the complexity of the structures in combination with the stepwise production routine, a detailed knowledge of the individual production steps is necessary. The basis for this is the application of process monitoring on the one hand and the evaluation and analysis of the data records obtained during processing on the other. One promising approach is to embed a digital twin in the production routine.[36] This approach is advantageous and relevant when distributed manufacturing entities are involved.

The production routine presented in Fig. 10 is realized in several iterations in order to progress from demonstrator structures to the final component set. The demonstrator structures incorporate critical design features that have already been identified in advance as technical and technological challenges from the perspective of both additive processing and subtractive processing. In additive processing, these include the manufacturability of overhangs, the resulting surface topographies (roughness) after processing and the removal of residual powder. With regard to subtractive processing, which is mainly realized by machining processes, small precision holes with high aspect ratios, heterogeneous material properties and the resulting alternating load on the super-hard cutting tools and the process stability from the context of permanently sharp tools represent the greatest challenges. In order to ensure process stability in particular,

DOI: 10.13009/EUCASS2025-710

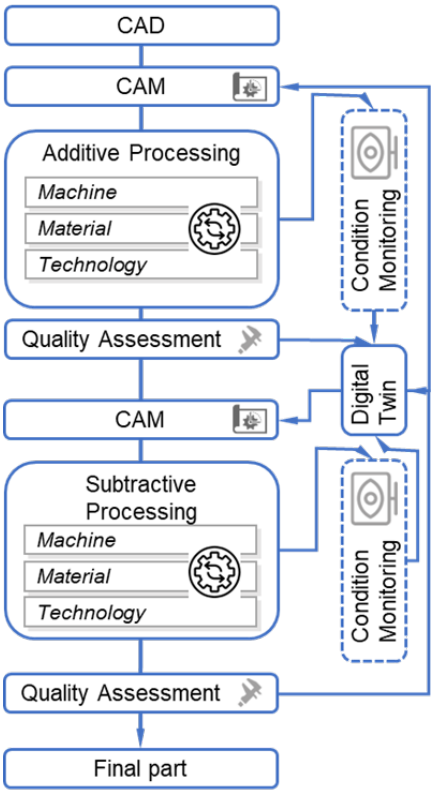

Figure 10: Process chain for the manufacturing routine

up-to-date process monitoring methods are used on the machines and processed in aggregated form. This data forms the basis for the application of the digital twin, as the holistic processing of the CuCr1Zr alloy can be regarded as fundamentally challenging.[37]

A modified EOS M290 (cf. Fig. 11a) machine is used for additive manufacturing of CuCr1Zr components via laser powder bed fusion (PBF-LB/M). This machine utilizes laser powers up to 900 W with a variable laser beam diameter between 95 and 900 μm. The machine is equipped with an EOState ExposureOT monitoring system to capture thermal emissions during the PBF-LB/M process. The monitoring system allows the detection of local differences in energy input resulting from critical geometrical features (i.e. overhangs).

A DMU Monoblock 65 FDS 2nd generation 5-axis machining center is used for subtractive processing (cf. Fig. 11b). This machine is equipped with a Siemens Sinumerik EDGE-device and an high precision in-spindle force measurement unit to monitor high frequency process data. From a tool perspective, it is known that tools with high hardness play an important role in maintaining cutting edge stability over the long term and that knowledge of the tool shape is also important. Tools with super-hard cutting materials made of cBN,[38] PCD[39] or even monocrystalline diamond due to their excellent tribological properties are relevant for this. The use of ductile cutting materials in the form of HSS due to the possibility of producing sharp cutting edges is also documented.[40]

3.2 Current manufacturing status

Besides arbitrary forms like cubes and spheres to conduct investigations on manufacturing process parameters for the additive and subtractive machining, critical design features from the test specimen components have been derived and manufactured (cf. Fig. 12a). These critical design features were selected with regards to critical overhang angles in cooling water manifolds in the in- and outlet sections, high aspect ratio openings e.g. for pressure probes, small cross-section cooling channel areas like the nozzle throat etc. The manufactured critical design features show persuasive dimensional accuracy both in the filigree and solid component regions after manufacturing (cf Fig. 12b). With minor improvements with respect to the component support structures, the additive manufacturing process for these components is regarded established.

DOI: 10.13009/EUCASS2025-710

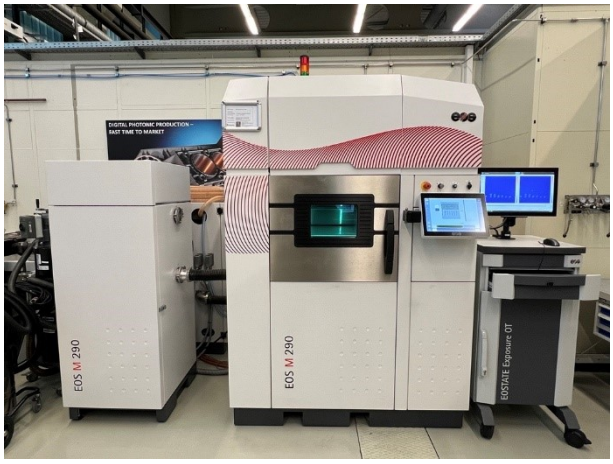

(a) EOS M290 for additive manufacturing

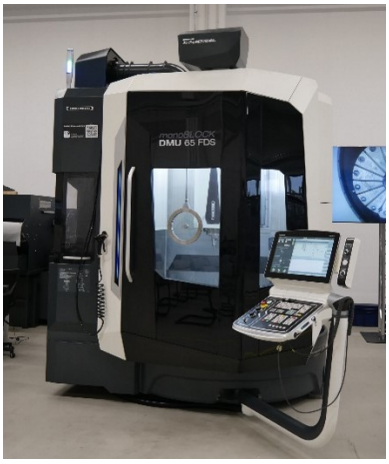

(b) DMU Monoblock 65 FDS 2^{nd} gen. for subtractive processing

Figure 11: Machine tool park for manufacturing of nozzle and spike

4. Test and verification approach

Currently, the test specimen is being additively manufactured, post-processed and quality checked by Fraunhofer ILT and IWU. After finalization of the manufacturing, the specimen's suitability for the test bench will be tested. At last, the specimen is expected to be hot-fired by DLR in order to conduct the envisaged experiments.

For the preparation of the test campaign, a comprehensive series of pre-tests are planned to be conducted (cf. Tab. 5), to ensure the reliability and performance of the cooling system and test specimen. These include a bubble leak test, which verifies the gas leak tightness of the cooling channels by detecting any potential leakage points under pressurized conditions. This is critical to maintain the integrity and safety of the system during operation. Additionally, a pressure test is carried out to confirm the structural load-bearing capacity of the cooling channels. This test ensures that the components can withstand the expected pressure levels without deformation or failure. The cooling system is further characterized by evaluating the required coolant mass flow within the limits of the available pressure budget. This step is essential to confirm that the cooling system can maintain adequate cooling efficiency during engine operation, ensuring that all components remain within their designated temperature ranges.

Table 5: Verification plan

Test	Verification aspect
Pre-Tests	
Bubble leak test	Proof of gas leak tightness of the cooling channels
Pressure test	Pressure load-bearing capacity of the cooling channels
Cooling system characterization	Required coolant mass flow is provided with available pressure budget
Engine test campaign	
Test objective #1	50%-Load-Point - Throttling to $\approx 50\,\%$
Test objective #2	100%-Load-Point - Adapted flow at design conditions - Load-bearing capability of the demonstrator - Heat load and pressure field distribution

Subsequently, the hot-gas tests will be conducted. The engine test campaign consists of two defined load points (cf. Tab. 6) to examine the performance and operational limits of the test specimen under various conditions. For the

DOI: 10.13009/EUCASS2025-710

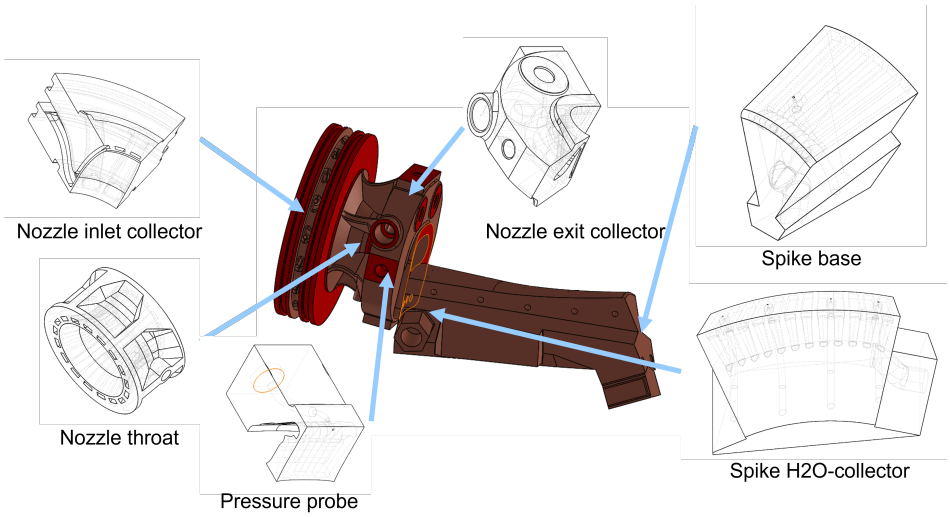

(a) CAD-model overview with origin of the CDFs

(b) First manufacturing iteration

Figure 12: Critical design features (CDFs) of the AM components

DOI: 10.13009/EUCASS2025-710

test objective # 1 (50%-Load-Point), the engine is throttled to approximately 50 % of its design thrust. This partial load condition allows for the assessment of system behavior at reduced performance levels.

For the test objective # 2 (100%-Load-Point), the system is operated under flow conditions that align with the original design specifications. This load point serves to validate the load-bearing capability of the test specimen under nominal conditions. Furthermore, detailed analysis is performed to assess the distribution of heat load and pressure fields across the system, providing insights into thermal and mechanical performance as well as identifying any areas that may require further optimization.

Table 6: Overview of Throttling regimes

Paramter	Load point #1	Load point #2
Thrust / kN (/%)	1.6 (≈ 50)	3.3 (≈ 100)
Chamber pressure / MPa	≈ 3.0	≈ 6.0
ROF / -	3.2	3.2
CH4 mass flow / kg/s	≈ 0.15	≈ 0.29
LOX mass flow / kg/s	≈ 0.48	≈ 0.94
Steady state test duration / s	10-20	10-20

It is expected, that the results of the test campaign will give more insight into the flow behavior of a clusterd aerospike nozzle under design and throttled conditions. Especially the detailed analysis into the flow behavior in the transition region from internal to external expansion is expected to reveal new insights.

5. Conclusion and Outlook

A test specimen for the flow investigation of a clustered aerospike nozzle segment has been designed for an existing LOX-methane combustion chamber and sea-level testing. Following considerations of the general design of the specimen, which led to a 1.5 module segment design, a banana-shaped internal expansion nozzle and the central spike were designed and harmonized to smoothen the expansion transition. A measurement approach measurement has been implemented for the determination of the pressure field on the spike surface, optical flow phenomena investigation and calorimetric heat load. In combination with two load point test scenarios, the throttling modes of chamber pressure reduction and deactivation for clustered aerospikes can be investigated with this specimen.

Additive and subtractive manufacturing methods will be used for the realization of the specimen. AM will be used to produce the water-cooled banana nozzle and the spike, for which in preparation critical design features have been build. Conventional manufacturing will be applied for the less complex components. After completion of the specimen and integration into the test bench, a test campaign will be conducted to verify the design methodology of the nozzles and obtain the desired measurements.

Acknowledgements

We would like to thank ESA for funding project THOMAS (4000142001/23/NL/MG) through a Technology Development Programme (TDE). Moreover, we thank our students André Dietz, Carl Theodor Petrich, Joshua Stoll and Charlie Weise, who contributed substantially to the progress of our research.

References

[1] H. Immich and R. Parsley. Plug engine systems for future launch vehicle applications. In *29th Joint Propulsion Conference and Exhibit*, Monterey, 1993.

[2] J. Ruf, R. Buck, A. Casiano, T. Diller, and J. Driscoll. The plume physics behind aerospike nozzle altitude compensation and slipstream effect. In *33rd Joint Propulsion Conference and Exhibit*, Seattle, 1997.

[3] G. Hagemann, M. M. Sippel, R. Sippel, H. Immich, and J. Van Den Braembussche. Advanced rocket nozzles. *Journal of Propulsion and Power*, pages 620–634, 1998.

DOI: 10.13009/EUCASS2025-710

[4] R. Silver. Advanced aerodynamic spike configurations - hot-ring investigations. Technical Report AFRPL-TR-67-246-Vol 2 AD-348 856, Rockwell International Corporation, Rocketdyne Division, 1967.

[5] Shannon D. Eilers, Matthew D. Wilson, Stephen A. Whitmore, and Zachary W. Peterson. Side-force amplification on an aerodynamically thrust-vectored aerospike nozzle. *Journal of Propulsion and Power*, 28(4):811–819, July 2012.

[6] StokesSpace. Update on hopper2: The hopper has landed. `https://www.stokespace.com/update-on-hopper2-the-hopper-has-landed/` [Accessed: February 2nd 2024].

[7] Giuseppe Scarlatella, Jacopo Guadagnini, Leonardo Paniccià, Gabriele De Zaiacomo, Martin Tajmar, Christian Bach, and Dario Pastrone. Assessment of mission capabilities of a reusable heavy-lift launch vehicle concept with aerospike engine. In *AIAA SCITECH 2024 Forum*. American Institute of Aeronautics and Astronautics, 2024.

[8] C. Bach, S. Schöngarth, B. Bust, M. Propst, J. Sieder-Katzmann, and M. Tajmar. How to steer an aerospike. In *International Astronautical Congress (IAC)*, 2018.

[9] F. Nasuti, M. Fiore, V. Messina, A. Valeriani, and D. Bianchi. Design and evaluation of aerospike nozzles for an upper stage application. In *Space Propulsion Conference*, 2021.

[10] Ralf Stark, Sebastian Bartel, Florian Ditsche, and Thomas Esch. Design Study of a 30kN LOX/LCH4 Aerospike Rocket Engine for Lunar Lander Application. In *Aerospace Europe Conference 2023 - 10th EUCASS - 9th CEAS*, 2023.

[11] Eric Besnard, Hsun Hu Chen, Tom Mueller, and John Garvey. Design, manufacturing and test of a plug nozzle rocket engine. In *38th AIAA/ASME/SAE/ASEE Joint Propulsion Conference and Exhibit*. American Institute of Aeronautics and Astronautics, July 2002.

[12] Eric Besnard, John Garvey, Tom Holleman, Tom Mueller, Hsun Hu Chen, and Hsin-Piao Chen. Student development and test of a gimbaled annular aerospike engine. In *38th AIAA/ASME/SAE/ASEE Joint Propulsion Conference and Exhibit*. American Institute of Aeronautics and Astronautics, July 2002.

[13] T. Bui, J. Barrows, M. Jacobsen, and D. Willoughby. Flight research of an aerospike nozzle using high power solid rockets. In *41st AIAA/ASME/SAE/ASEE Joint Propulsion Conference & Exhibit*, 2005.

[14] J. Dennis, D. Lichtenstein, and S. A. Whitmore. Design of a n2o/htpb hybrid rocket motor utilizing a toroidal aerospike nozzle. In *48th AIAA Aerospace Sciences Meeting Including the New Horizons Forum and Aerospace Exposition*, Florida, 2010.

[15] NextAero. Projectx, 2025. `https://nextaero.com.au/index.php/engine-progress/projectx/` [Accessed May 2025].

[16] F. Rossi, Z. Sápi, N. Palumbo, A. Demediuk, and Miguel Ampudia. Manufacturing and hot-fire test campaign of the demop1 aerospikeengine demonstrator. In *Space Propulsion Conference 2022*, 2022.

[17] Maximilian Buchholz, Samira Gruber, Axel Marquardt, Lukas Seifert, Alex Selbmann, Christoph Leyens, Martin Tajmar, and Christian Bach. Design and test of an additively manufactured 500 n aerospike engine. In *Space Propulsion Conference*, 2022.

[18] Tim Dorau, Martin Propst, Samira Gruber, Alex Selbmann, Adheena Gana Joseph, Jan Sieder-Katzmann, Maximilian Buchholz, Kamil Sobczak, Sebastian Solleri, Martin Tajmarj, and Christian Bach. Development of an additively manufactured hydrogen peroxide/kerosene 6kn aerospike breadboard engine. In *72nd International Astronautical Congress (IAC), Dubai, UAE*, 2021.

[19] Martin Propst, Tim Dorau, Adheena Gana Joseph, Jan Sieder-Katzmann, Maximilian Buchholz, Samira Gruber, Alex Selbmann, Filofteia-Laura Toma, Kamil Sobczak, Tobiasz Mayer, Sebastian Soller, Simon Hyde, Martin Tajmar, and Christian Bach. Evaluation of Hot-Fire Test Campaign of a 6 kN H2O2/Kerosene Aerospike Engine Demonstrator. In *11th European Conference for AeroSpace Sciences 2025 - EUCASS*, Rome, Italy June 30th - July 4th, 2025.

[20] RocketStar. Rocket engine development, 2025. `https://rocketstar.nyc/` [Accessed May 2025].

[21] Product: Aerospike technology. `https://pangeaaerospace.com/products/`, [Accessed: February 15th 2023].

DOI: 10.13009/EUCASS2025-710

[22] Matthew Baker, Eric Besnard, and Jay Clark. CFD analyses in support of the flight test of a multi-chamber LOX/ethanol aerospike engine. In *43rd AIAA/ASME/SAE/ASEE Joint Propulsion Conference and Exhibit*. American Institute of Aeronautics and Astronautics, July 2007.

[23] Eric Berger. Firefly returns from the dead with a larger rocket and lunar aspirations, 2019. https://arstechnica.com/science/2019/02/firefly-returns-from-the-dead-with-a-larger-rocket-and-lunar-aspirations/ Accessed 17 June 2025.

[24] H. F. R. Schöyer. Thrust vector control for (clustered modules) plug nozzles: Some considerations. *Journal of Propulsion and Power*, 16(2):196–201, March 2000.

[25] Michele Ferlauto, Andrea Ferrero, Matteo Marsicovetere, and Roberto Marsilio. Differential throttling and fluidic thrust vectoring in a linear aerospike. *International Journal of Turbomachinery, Propulsion and Power*, 6(2):8, April 2021.

[26] Klaus Schäfer and Anja Frank. European test center dlr lampoldshausen, shaping the future. In *Space Propusion Conference 2016*, 2016.

[27] Joachim Sender, Dmitry Suslov, Justin Hardi, and Michael Oschwald. Role of subscale tests for rocket engine technology development and verification. *proceedings-Space Propulsion 2018*, 2018.

[28] Richard Arnold. *Experimentelle Untersuchungen zur Filmkühlung in Raketenbrennkammern*. Cuvillier Verlag, 2008.

[29] Dmitry Suslov, Jan C Deeken, and Michael Oschwald. Experimental investigation of the film cooling efficiency in a high pressure lox/h2 combustion chamber. In *61. Deutscher Luft- und Raumfahrtkongress (DLRK)*, 2012.

[30] Dmitry Suslov, Oskar Haidn, and R. Arnold. Film cooling in a high-pressure subscale combustion chamber. *Journal of Propulsion and Power*, Vol. 26(no. 3):428–438, 2010.

[31] Michael Börner. Experimentelle untersuchung der laserinduzierten zündung von kryogenen flüssigkeitsraketenbrennkammern. Technical report, RWTH Aachen, 2022.

[32] Gianfranco Angelino. Approximate method for plug nozzle design. *AIAA Journal*, 2(10):1834–1835, October 1964.

[33] Takashi Ito and Kozo Fujii. Numerical analysis of the base bleed effect on the aerospike nozzles. In *40th AIAA Aerospace Sciences Meeting and Exhibit*. American Institute of Aeronautics and Astronautics, January 2002.

[34] Alexander Ponomarenko. Rocket propulsion analysis v1.2.9 standard, 2017. https://www.rocket-propulsion.com/index.htm [released: January 12th 2017].

[35] Brandenburger. S 5000®, 2025. https://brandenburger-isoliertechnik.com/produkte/ablationsmaterial/s-5000 [Accessed April 2025].

[36] Albrecht Hänel, André Seidel, Uwe Frieß, Uwe Teicher, Hajo Wiemer, Dongqian Wang, Eric Wenkler, Lars Penter, Arvid Hellmich, and Steffen Ihlenfeldt. Digital twins for high-tech machining applications—a model-based analytics-ready approach. *Journal of Manufacturing and Materials Processing*, 5(3):80, July 2021.

[37] Yuchao Bai, Cuiling Zhao, Yu Zhang, Jie Chen, and Hao Wang. Additively manufactured cucrzr alloy: Microstructure, mechanical properties and machinability. *Materials Science and Engineering: A*, 819:141528, July 2021.

[38] Dongqian Wang, Lu Yin, Albrecht Hänel, Uwe Teicher, Lars Penter, André Seidel, Simon Harst, and Steffen Ihlenfeldt. Cutting performance of binderless nano-polycrystalline cbn and pcbn milling tools for high-speed milling of hardened steel. *Ceramics International*, 49(22):34757–34773, November 2023.

[39] U. Teicher, S. Pirl, A. Nestler, A. Hellmich, and S. Ihlenfeldt. Surface roughness and its prediction in high speed milling of aluminum alloys with pcd and cemented carbide tools. *MM Science Journal*, 2019(04):3136–3141, November 2019.

[40] Aklilu Getachew Tefera, Devendra Kumar Sinha, and Gaurav Gupta. Experimental investigation and optimization of cutting parameters during dry turning process of copper alloy. *Journal of Engineering and Applied Science*, 70(1), November 2023.